Inorganic Chemistry

Article

pubs.acs.org/IC

Synthesis, Magnetism, and ^{57}Fe Mössbauer Spectroscopic Study of a Family of [Ln_3Fe_7] Coordination Clusters (Ln = Gd, Tb, and Er)

Ghulam Abbas,[†,‡] Yanhua Lan,[†] Valeriu Mereacre,[†] Gernot Buth,[§] Moulay T. Sougrati,[∥] Fernande Grandjean,[∥] Gary J. Long,*[,⊥] Christopher E. Anson,[†] and Annie K. Powell*[,†,¶]

[†]Institut für Anorganische Chemie, Karlsruhe Institute of Technology, Engesserstrasse 15, D-76131 Karlsruhe, Germany

[§]Institut für Synchrotronstrahlung and [¶]Institut für Nanotechnologie, Karlsruhe Institute of Technology, Hermann-von-Helmholtz-Platz 1, D-76344 Eggenstein-Leopoldshafen, Germany

[∥]Department of Physics, University of Liège, B-4000 Sart-Tilman, Belgium

[⊥]Department of Chemistry, Missouri University of Science and Technology, University of Missouri, Rolla, Missouri 65409-0010, United States

Supporting Information

ABSTRACT: The reaction of *N*-methydiethanolamine ($mdeaH_2$), benzoic acid, $FeCl_3$, and $Ln(NO_3)_3{\cdot}6H_2O$ or $LnCl_3{\cdot}xH_2O$ yields a series of decanuclear coordination clusters, $[Ln_3Fe_7(\mu_4\text{-}O)_2(\mu_3\text{-}OH)_2(mdea)_7(\mu\text{-benzoate})_4(N_3)_6]{\cdot}4MeCN{\cdot}H_2O$, where Ln = Gd^{III} (**1**) or Tb^{III} (**2**), and $[Er_3Fe_7(\mu_4\text{-}O)_2(\mu_3\text{-}OH)_2(mdea)_7(\mu\text{-benzoate})_4(N_3)_5(MeOH)]Cl{\cdot}7.5H_2O{\cdot}11.5MeOH$ (**3**). The isostructural compounds **1**−**3** all crystallize isotypically in the triclinic space group $P\bar{1}$ with $Z = 2$, as does the previously reported dysprosium analogue **4**. Six of the Fe^{III} ions are *pseudo*octahedrally coordinated, whereas the seventh has a trigonal-bipyramidal coordination geometry. Temperature-dependent direct-current magnetic susceptibility studies indicate that intracluster antiferromagnetic interactions are dominant in **1**−**3**. The frequency-dependent out-of-phase (χ'') alternating-current susceptibility reveals that **2** undergoes a slow relaxation of its magnetization, presumably resulting from anisotropy of the Tb^{III} ions. Between 30 and 295 K, the ^{57}Fe Mössbauer spectra reveal paramagnetic behavior with six partially resolved quadrupole doublets, one for the trigonal-bipyramidal Fe^{III} site and five for the six *pseudo*octahedral Fe^{III} sites. The Mössbauer spectra of **2** and **3** obtained between 3 and 30 K are consistent with the presence of Fe^{III} intracluster antiferromagnetic coupling with slow magnetic relaxation relative to the Larmor precession time. Further, the observed changes in the effective magnetic field values in the spectra measured at 3 K with increasing applied field are consistent with the effect of the local spin polarization along the applied magnetic field direction, a behavior reminiscent of antiparallel spin-coupled iron molecular paramagnetic systems.

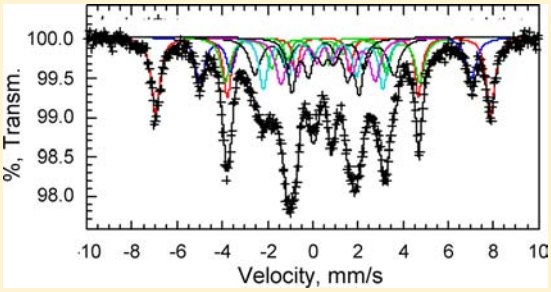

1. INTRODUCTION

The study of high-nuclearity coordination clusters has attracted much attention in recent years with the discovery that such molecules can display the phenomenon of single-molecule magnets (SMMs),[1] providing a significant boost to efforts on developing synthetic routes to such molecules as well as understanding the relationship between their molecular structures and magnetic properties. The characteristic magnetic behavior of SMMs is that a slow relaxation of the magnetization of purely molecular origin is observed, and this usually derives from the combination of a nonzero ground-state spin (S) and the large and negative magnetoanisotropy of an Ising and easy-axis type, as can be quantified by an overall molecular axial zero-field-splitting parameter D.[1,2] These molecules behave as magnets below a blocking temperature (T_B) and exhibit hysteresis in magnetization versus direct-current (dc) field scans. These hysteresis loops display increasing coercivity with decreasing temperature and increasing field sweep rates, which is taken as the characteristic signature of SMMs. Recently, particular attention has been directed toward synthesizing heterometallic complexes featuring both 3d and 4f block elements, and the distinct coordination behaviors of the different metal ions have been observed in a large number of stunningly beautiful complexes.[3] Although incorporation of lanthanide ions represents an effective way of introducing magnetic anisotropy into a coordination cluster because of the large orbital contributions from such ions, a major drawback is the weak coupling between the molecular building blocks.[4] In general, the coupling between atomic spins arising from unpaired d electrons is typically on the order of 10−100 K, whereas the coupling between atomic spins arising from unpaired f electrons is ca. 1 K and the coupling between atomic spins arising from unpaired d and f electrons is expected to be less than 10 K. The first investigation of the magnetic properties of a heterometallic 3d−4f complex was reported by Gatteschi et al., who thoroughly characterized and

Received: April 28, 2013
Published: October 3, 2013

   dx.doi.org/10.1021/ic401011d | *Inorg. Chem.* 2013, 52, 11767−11777

analyzed two Cu−Gd complexes.[5] As a result of this, great attention was paid to synthesizing coordination complexes of [Cu−Ln],[6] [Mn−Ln],[7] [Co−Ln],[8] and [Ni−Ln];[9] however, there are comparatively few reports of [Fe−Ln][10] complexes.

Chelating ligands featuring alkoxy donor groups have been widely employed in the synthesis of high-nuclearity clusters because they can both be part of chelate rings and form efficient bridges to further metal centers.[11] Aminopolyalcohol ligands have the additional advantage of possessing hard-donor oxygen, tending to bind preferentially to oxophilic lanthanide ions, with the soft-donor nitrogen binding preferentially to transition-metal ions. This combined with the deprotonated alcohol arms of these ligands bridging metal centers favors the formation of high-nuclearity coordination clusters. As a continuation of our work on the synthesis of iron lanthanide ion clusters,[10] we recently reported on the properties of $[Dy_3Fe_7(\mu_4\text{-}O)_2(\mu_3\text{-}OH)_2(mdea)_7(\mu\text{-benzoate})_4(N_3)_6]\cdot 2H_2O\cdot 7CH_3OH$,[10l] where we used *N*-methyldiethanolamine ($mdeaH_2$) as a ligand. Although use of this ligand in the coordination chemistry of transition-metal ions has been reported recently,[11a,12] examples of $mdeaH_2$ acting as a ligand in 3d−4f heterometal clusters are still rare.[13] Our previous study on $[Dy_3Fe_7(\mu_4\text{-}O)_2(\mu_3\text{-}OH)_2(mdea)_7(\mu\text{-benzoate})_4(N_3)_6]\cdot 2H_2O\cdot 7CH_3OH$[10l] showed that the molecule undergoes slow relaxation of its magnetization. The effective energy barrier, U_{eff}, of 33.4 K for this relaxation is the highest yet reported for a Fe^{III} 4f SMM and the fourth highest energy barrier yet reported for any 3d−4f SMM.[6e,7i,13] Although many SMMs containing Fe^{III} are known,[14] they tend to have low effective energy barriers, and it is thus likely that the height of the energy barrier in the aforementioned $\{Dy_3Fe_7\}$ coordination cluster mainly results from the contributions of the single-ion anisotropies of the Dy^{III} ions, as we previously demonstrated in the case of Mn^{III}−Dy^{III} SMMs.[13]

^{57}Fe Mössbauer spectroscopy has been a widely used technique to determine the oxidation levels and spin states,[15] local moments at the iron nuclei and spin-relaxation dynamics,[16] structural changes in the coordination sphere,[17] and anisotropy not only of the studied isotope but also of elements interacting with this isotope.[10p,q] Recently, we began exploring ^{57}Fe Mössbauer spectroscopy as a means of probing the spin structure of coordination clusters such as $Fe^{III}_7Ln^{III}_4$[10o] and Fe_{16},[12g] because it is well-known that the description of the spin structures of many electron systems with antiparallel spins is at best difficult using numerical or modeling techniques.[18] The effect of ligand substitution on the interaction between the dysprosium and iron ions in $\{Fe_2Dy_2\}$ clusters has also been investigated by means of ^{57}Fe Mössbauer spectroscopy.[10q] The results indicate that Dy^{III}−Fe^{III} interactions and the shape anisotropy are controlled by a combination of the crystal-field interaction and applied magnetic field. Using ^{57}Fe Mössbauer spectroscopy, different examples of coordination compounds with different topologies containing Fe^{III} and Ln^{III} ions (Dy^{III} and Tb^{III}) were analyzed in terms of spotting the difference between the anisotropies of various lanthanides.[10r] It could be shown how in the same crystal-field environmental Dy and Tb ions show different degrees of anisotropy and how this anisotropy can be qualitatively detected using this spectroscopy.

With these results in mind, we have extended the work on the $\{Ln_3Fe_7\}$ coordination cluster system that we originally reported for the Dy^{III} congener to the compounds $[Ln_3Fe_7(\mu_4\text{-}O)_2(\mu_3\text{-}OH)_2(mdea)_7(\mu\text{-benzoate})_4(N_3)_6]\cdot 4MeCN\cdot H_2O$, where Ln = Gd^{III} (**1**) and Tb^{III} (**2**), and $[Er_3Fe_7(\mu_4\text{-}O)_2(\mu_3\text{-}OH)_2(mdea)_7(\mu\text{-benzoate})_4(N_3)_5(MeOH)]Cl\cdot 7.5H_2O\cdot 11.5MeOH$ (**3**), which are all isostructural to the $\{Dy_3Fe_7\}$ compound (**4**) and crystallize isotypically with it. We describe the synthesis, structures, and magnetic and Mössbauer spectral properties of these new compounds and compare the results with those of the $\{Dy_3Fe_7\}$ compound.

2. EXPERIMENTAL SECTION

2.1. Synthesis. Unless otherwise stated, all reagents were obtained from commercial sources and were used as received without further purification. All reactions were carried out under aerobic conditions. Elemental analyses for carbon, hydrogen, and nitrogen were performed using an Elementar Vario EL analyzer. IR spectra were measured on a Perkin-Elmer Spectrum One spectrometer as KBr disks.

*Preparation of $[Gd_3Fe_7(\mu_4\text{-}O)_2(\mu_3\text{-}OH)_2(N_3)_6(mdea)_7(PhCO_2)_4]\cdot 4MeCN\cdot H_2O$ (**1**).* A solution of *N*-methyldiethanolamine ($mdeaH_2$; 0.148 g, 1.25 mmol) in MeCN (20 mL) was added dropwise over 20 min to a stirred solution of $Gd(NO_3)_3\cdot 6H_2O$ (0.113 g, 0.25 mmol), benzoic acid (0.030 g, 0.25 mmol), $FeCl_3$ (0.040 g, 0.25 mmol), and NaN_3 (0.051 g, 0.75 mmol) in MeCN (20 mL). The mixture was heated under reflux for 1 h, after which it was cooled to room temperature and then allowed to stand undisturbed in a sealed vial. Orange needles of **1** suitable for X-ray crystallography were obtained after 15 days. These were collected by filtration, washed with MeCN, and dried in air. Yield: 40%. Crystals for X-ray crystallography were maintained under mother liquor to avoid solvent loss.

Anal. Calcd (found) for $C_{63}H_{105}Gd_3Fe_7N_{25}O_{29}$, corresponding to $[Gd_3Fe_7(\mu_4\text{-}O)_2(\mu_3\text{-}OH)_2(N_3)_6(mdea)_7(PhCO_2)_4]\cdot 2H_2O$: C, 30.01 (29.91); H, 4.12 (3.92); N, 13.89 (13.79). IR (KBr): ν 3424 (w), 2856 (w), 2059 (vs), 1625 (m), 1597 (m), 1547 (m), 1447 (w), 1399 (m), 1084 (s), 1026 (w), 1000 (w), 998 (m), 721 (m), 650 (w), 577 (w), 490 (w) cm^{-1}.

*Preparation of $[Tb_3Fe_7(\mu_4\text{-}O)_2(\mu_3\text{-}OH)_2(N_3)_6(mdea)_7(PhCO_2)_4]\cdot 4MeCN\cdot H_2O$ (**2**).* The preparation was similar to that for **1** but with $Gd(NO_3)_3\cdot 6H_2O$ replaced by $Tb(NO_3)_3\cdot 6H_2O$ (0.114g, 0.25 mmol). Yield: 45%. Anal. Calcd (found) for $C_{67}H_{105}Tb_3Fe_7N_{27}O_{26}$, corresponding to $[Tb_3Fe_7(\mu_4\text{-}O)_2(\mu_3\text{-}OH)_2(N_3)_6(mdea)_7(PhCO_2)_4]\cdot 2MeCN$: C, 31.28 (31.63); H, 4.11 (3.81); N, 14.70 (14.35). IR (KBr): ν 3421 (w), 2861 (m), 2059 (vs), 1593 (s), 1546 (vs), 1458 (w), 1400 (s), 1332 (w), 1287(w), 1261 (w), 1144 (w), 1086 (s), 1026 (m), 999 (m), 897 (m), 721 (s), 654 (w), 578 (m), 491 (w) cm^{-1}.

*Preparation of $[Er_3Fe_7(\mu_4\text{-}O)_2(\mu_3\text{-}OH)_2(N_3)_5(MeOH)(mdea)_7(PhCO_2)_4]Cl\cdot 11.5MeOH\cdot 7.5H_2O$ (**3**).* The preparation was similar to that for **1** but with $Gd(NO_3)_3\cdot 6H_2O$ replaced by $ErCl_3\cdot xH_2O$ (0.067 g) and MeOH as the solvent. Yield: 44%. Anal. Calcd (found) for $C_{64}H_{141}ClEr_3Fe_7N_{25}O_{29}$, corresponding to $[Er_3Fe_7(\mu_4\text{-}O)_2(\mu_3\text{-}OH)_2(N_3)_5(MeOH)(mdea)_7(PhCO_2)_4]Cl\cdot 2H_2O$: C, 29.83 (29.73); H, 4.19 (3.83); N, 11.96 (11.95). IR (KBr): ν 3438 (w), 2921 (w), 2856 (w), 2059 (vs), 1593 (m), 1548 (s), 1455 (w), 1400 (m), 1287 (w), 1087 (m), 1026 (w), 1000 (w), 897 (m), 721 (m), 659 (w), 579 (w), 493 (w) cm^{-1}.

2.2. X-ray Crystallography. X-ray data were collected on a Bruker SMART Apex (**1** and **2**) or an Oxford SuperNova (**3**) diffractometer. For compound **1**, it was necessary to use synchrotron radiation, and the data set was measured on the SCD beamline at the ANKA synchrotron source, Karlsruhe, using silicon-monochromated radiation of wavelength 0.80000 Å; for **2** and **3**, graphite-monochromated Mo Kα radiation from conventional sources was adequate. The anomalous scattering factors f' and f'' for the structure of **1** were calculated by the method of Brennan and Cowan,[19] as implemented in http://skuld.bmsc.washington.edu/scatter/AS_periodic.html

All of the structures twin by a 180° rotation about c^*, and data were integrated allowing for this twinning and corrected for absorption. The structures were solved using direct methods, followed by full-matrix least-squares refinement against F^2 (all data) in HKLF 5 format using *SHELXTL*.[20] In the case of **2**, the twinning problems (see the Results and Discussion section) were such that it was only possible to refine the metal atoms anisotropically. The structure therefore cannot be described as fully refined, even though the resulting *R* factors are respectable. Nonetheless, the structure analysis is sufficient to show that

Table 1. Crystal Data for 1−3

	1	2[a]	3	4[10l]
formula	$C_{71}H_{113}Fe_7Gd_3N_{20}O_{27}$	$C_{71}H_{113}Fe_7N_{29}O_{27}Tb_3$	$C_{65.5}H_{124}ClEr_3Fe_7N_{22}O_{36}$	$C_{70}H_{131}Dy_3Fe_7N_{25}O_{35}$
fw, g mol^{-1}	2667.60	2672.53	2724.05	2761.45
cryst syst	triclinic	triclinic	triclinic	triclinic
space group	$P\bar{1}$	$P\bar{1}$	$P\bar{1}$	$P\bar{1}$
a/Å	14.444(2)	14.366(2)	14.1532(2)	14.2482(17)
b/Å	17.383(3)	17.128(2)	17.1938(4)	17.446(2)
c/Å	21.268(3)	21.209(3)	21.1108(4)	21.224(2)
α/deg	91.229(3)	90.572(3)	90.405(2)	90.430(2)
β/deg	93.576(3)	93.727(3)	92.299(1)	92.445(2)
γ/deg	98.440(3)	97.761(3)	98.269(1)	98.504(2)
V/Å^3	5269.1(13)	5173.7(13)	5079.33(17)	5212.4(11)
Z	2	2	2	2
T/K	150(2)	100(2)	100(2)	100(2)
F(000)	2664		2724	
D_c/Mg m^{-3}	1.681		1.781	
λ/Å	0.80000	0.71073	0.71073	0.71073
μ/mm^{-1}	3.921		3.530	
reflns measd	44236		76690	
unique reflns	20831		25817	
R_{int}	0.0546		0.0350	
data with $I \geq 2\sigma(I)$	17657		18487	
wR2 (all data)	0.2492		0.1863	
S (all data)	1.051		1.080	
R1 [$I \geq 2\sigma(I)$]	0.0910		0.0661	
param/restraints	1203/69		1196/41	
biggest diff peak/hole/(e Å^{-3})	+3.14/−3.25		+3.96/−1.97	
CCDC	849601		849602	729433

[a]The structure of **2** was not fully refined. The unit cell parameters are included here for comparison with those of **1** and **3** and also **4** from ref 10l.

2 is isostructural with its analogues **1** and **4**. Compound **3** is closely isostructural to **1**, **2**, and **4**, but it was found that the ligands on Fe(6) and Fe(7) could be better refined as disordered superpositions of azide and MeOH, with the ligands on these two sites having an overall composition of one azide and one MeOH, requiring one singly charged counteranion (a chloride) to balance the charge (see the Results and Discussion section). For compounds **1** and **3**, all ordered non-hydrogen atoms were refined anisotropically with hydrogen atoms placed in calculated positions. Similarity restraints were applied to the geometrical and/or thermal parameters within disordered groups where necessary. The assignment of all of the iron centers as Fe^{III} and the assignment of bridging oxygen atoms as oxide or hydroxide were established by charge-balance considerations, bond valence sum calculations,[21] and inspection of the metric parameters.

Crystallographic data and structure refinements for **1** and **3** are summarized in Table 1, which includes the unit cell parameters for **2** and **4**[10l] for comparison. Crystallographic data (excluding structure factors) for the structures of **1** and **3** have been deposited with the Cambridge Crystallographic Data Centre as supplementary publications CCDC 849601 and 849602. The structure of **4** was previously deposited[10l] as CCDC 729433. These data can be obtained free of charge via www.ccdc.cam.ac.uk/data_request/cif or by e-mailing data_request@ccdc.cam.ac.uk or contacting The Cambridge Crystallographic Data Centre, 12 Union Road, Cambridge CB2 1EZ, U.K. (fax +44 1223 336033).

2.3. Magnetic Susceptibility. Measurements were obtained on a Quantum Design SQUID MPMS-XL magnetometer. Measurements were performed on polycrystalline samples of 15.2 (**1**, Gd_3Fe_7), 6.9 (**2**, Tb_3Fe_7), and 10.1 (**3**, Er_3Fe_7) mg. The samples of Tb_3Fe_7 and Er_3Fe_7 were dispersed in Apiezon grease to avoid torquing of the molecules. Alternating-current (ac) susceptibility measurements were performed with an oscillating ac field of 3 Oe and ac frequencies ranging from 1 to 1500 Hz. M vs H measurements were performed at 100 K to check for the presence of ferromagnetic impurities; none were observed. The magnetic data were corrected for the sample holder and diamagnetic contribution.

2.4. Mössbauer Spectroscopy. The Mössbauer spectral absorbers contained 22−24 mg cm^{-2} of finely powdered **1**−**3** dispersed in boron nitride. The spectra were obtained both between 3 and 295 K without a field and at 3 K using transverse applied magnetic fields of up to 5 T, equipped with a constant acceleration spectrometer with a rhodium-matrix cobalt-57 source and was calibrated at 295 K with α-iron powder. The isomer shifts are given relative to α-iron powder at 295 K. The statistical errors for the spectral fits discussed below are given in parentheses; the absolute errors are estimated to be approximately twice as large as the statistical errors.

3. RESULTS AND DISCUSSION

3.1. Synthesis. In the work reported here, the reaction between $Ln(NO_3)_3{\cdot}6H_2O$, benzoic acid, $FeCl_3$, NaN_3, and $mdeaH_2$ in a molar ratio of 1:1:1:3:6 in MeCN gave a red solution, from which orange crystals of **1** and **2** crystallized in good yield after 2 weeks. However, the erbium analogue (**3**) could only be obtained by the reaction between $ErCl_3{\cdot}xH_2O$, benzoic acid, $FeCl_3$, NaN_3, and $mdeaH_2$ in the same molar ratio in a methanol (MeOH) solution. When the reaction was carried out in methyl cyanide (MeCN), as for **1** and **2**, no pure product could be isolated.

3.2. Crystal Structures. X-ray crystallographic analysis of compounds **1**−**3** showed that crystals of these Ln_3Fe_7 compounds, whether obtained from MeOH or MeCN, all crystallize in the triclinic space group $P\bar{1}$ with $Z = 2$, isotypically to the previously reported Dy_3Fe_7 derivative **4**.[10l] They are all closely isostructural. As previously discussed,[10l] within this structure type, the molecular 2-fold axes are aligned almost exactly perpendicular to the {001} plane and the crystal structure as a whole has *pseudo*-2-fold symmetry in this direction. As a consequence, all of the crystals studied showed twinning by a

dx.doi.org/10.1021/ic401011d | Inorg. Chem. 2013, 52, 11767−11777

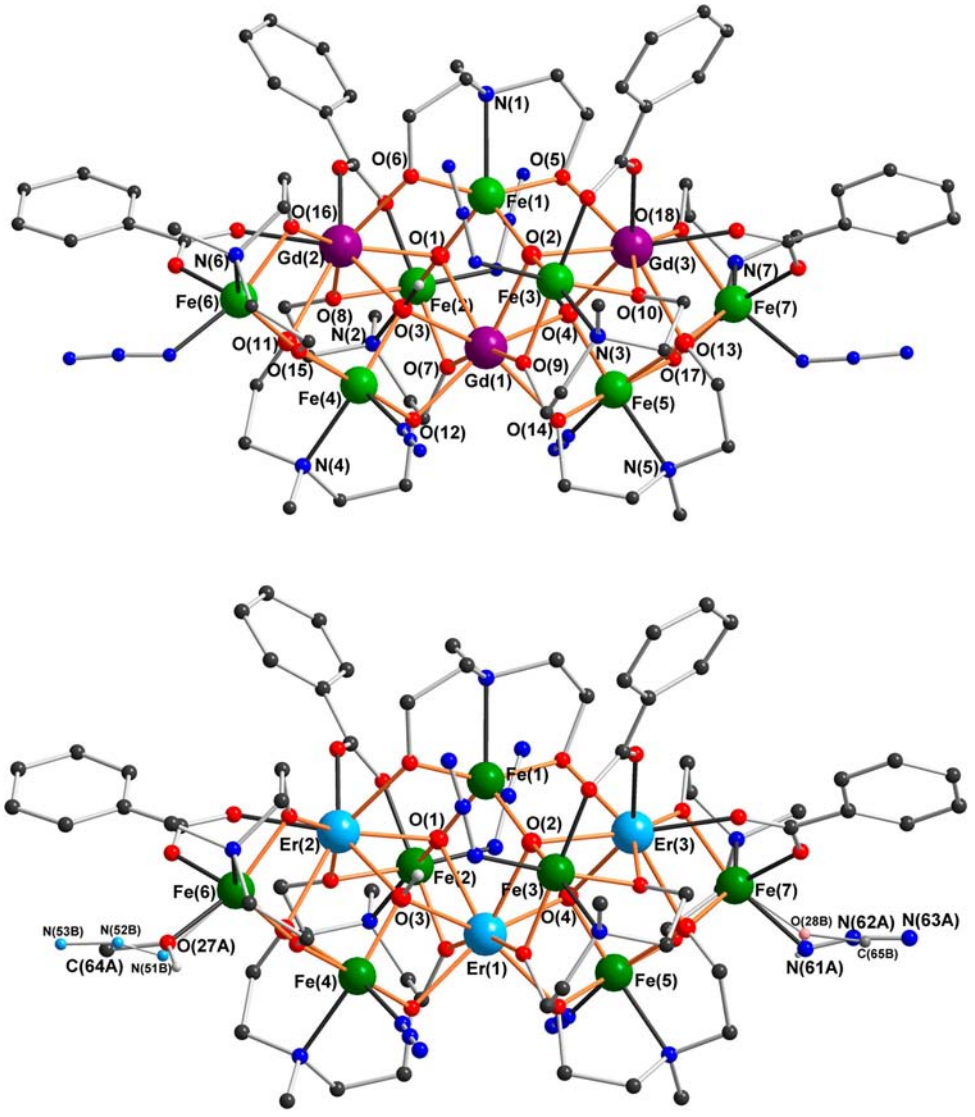

Figure 1. Molecular structures of **1** (top) and **3** (bottom). Organic hydrogen atoms and minor disorder components of $(mdea)^{2-}$ ligands are omitted for clarity; the minor components of the azide/MeOH disorder in **3** are shown as smaller, paler atoms.

180° rotation about c^*. Because α is close to 90° (90.4–91.2°), the two reciprocal lattices are nearly coincident, giving rise to many overlapped reflections, and in many cases, the pairs of reflections from the two twin components are not well-defined, appearing streaky. Thus, care was needed to find crystals minimizing these problems and for which the above twinning was relatively clean to allow for successful integration of the data and modeling of the twinning. For compounds **1** and **3**, it was possible to obtain data sets such that the respective structures could be refined (against data in HKLF 5 format) to an acceptable standard, although for **1** it proved necessary to use a very small crystal and, therefore, synchrotron radiation. For **2**, the best data set obtained was only sufficient for anisotropic refinement of the metal atoms because, as a result of the twinning problems, the carbon, nitrogen, and oxygen atoms could only be refined isotropically. Although this refinement is therefore not of fully publishable standard and only the unit cell parameters are listed in Table 1, it was sufficient to establish that **2** is indeed isostructural with the other compounds (Figure S1 in the Supporting Information, SI).

The nitrogen atoms of the terminal azide ligands in the complexes generally refined unexceptionally with the major axes of the three thermal ellipsoids within a given ligand essentially parallel to each other but perpendicular to the N–N–N direction. For **3**, however, the thermal ellipsoids of the central nitrogen atoms of the two azides bonded to Fe(6) and Fe(7) were elongated along the ligand axes. Furthermore, the microanalytical data for **3** were consistently different from those of the other analogues, with significantly lower values for nitrogen indicating replacement of one azide by chloride in the overall formulation. Modeling the two azides in question as disordered superpositions of azide and (neutral) MeOH ligands, such that the sums of the relative occupancies amounted to one azide and one MeOH, led to a satisfactory refinement. The chloride counterion necessary to balance the charge was found to be disordered over two positions among the lattice water molecules, with disorder resulting from the different hydrogen-bonding requirements of azide and MeOH.

The structures of Gd_3Fe_7 (**1**) and Er_3Fe_7 (**3**) are shown in Figure 1. Because compounds **1**–**3** are all isostructural or closely so with the Dy_3Fe_7 analogue **4**, the structure of which has

dx.doi.org/10.1021/ic401011d | *Inorg. Chem.* 2013, 52, 11767–11777

previously been described in detail,[10l] only the salient features of the cluster cores will be noted here. The molecules have an idealized (i.e., noncrystallographic) 2-fold axis passing through Ln(1), Fe(1), and N(1). Within the central core, each of the seven crystallographically inequivalent Fe^{III} cations is chelated by a doubly deprotonated $(mdea)^{2-}$ ligand, the two oxygen atoms of which each form bridges to other metal centers. The two $(\mu_4\text{-}O)^{2-}$ ligands O(1) and O(2) each bridge between two iron and two lanthanide centers. The resulting distorted tetrahedral $\{Fe_2Ln_2(\mu_4\text{-}O)\}$ units share one edge along Fe(1)···Ln(1). The two Ln···Ln edges of these tetrahedra are each further bridged by a hydroxo ligand, O(3) or O(4), which both form $(\mu_3\text{-}OH)^-$ bridges to a further iron center, The final two μ_3-bridges are provided by the alkoxo oxygen atoms O(11) and O(13) from two $(mdea)^{2-}$ ligands, while the remaining 12 $(mdea)^{2-}$ oxygen atoms each form a μ-OR bridge between the iron to which their respective ligand chelates and one other metal center to give further Fe···Ln and Fe···Fe bridges.

The Fe−O−Ln, Ln−O−Ln, and Fe−O−Fe angles are in the range 96−112° apart from Fe(1)−O(1)−Fe(2) and Fe(1)−O(2)−Fe(3), which are both over 140°. The four benzoate ligands form syn,syn bridges between an iron and a lanthanide center. These along with the azido ligands complete the peripheral ligand spheres. Fe(1) has a five-coordinate trigonal-bipyramidal NO_4 environment in which the two alkoxo oxygen atoms O(5) and O(6) occupy the axial sites, whereas N(1) and the two oxo ligands define the equatorial positions. The coordination spheres of the other iron centers can be described in terms of a distorted *cis*-N_2O_4 octahedral environment. The three lanthanide centers are all eight-coordinate with approximate square-antiprismatic geometries.

3.3. Magnetic Studies. The temperature dependence of the dc magnetic susceptibilities of compounds **1**−**3** shows similar thermal evolution in the temperature range 1.8−300 K (Figure 2). The magnetic data are summarized in Table 2. The χT product values at room temperature are lower than the expected value for systems containing seven Fe^{III} ions ($S = {}^5/_2$, $g = 2$, and $C = 4.375$ cm^3 K mol^{-1}) and the three respective Ln^{III} ions. Within the structures, the Fe^{III} ions are linked by double oxygen bridges with Fe−O−Fe angles in the range 100−145°. Magneto-structural correlations for oxygen-bridged Fe^{III} complexes[22] suggest that these bridges should mediate antiferromagnetic interactions within the range of −20 to −80 K, thus leading to lower values than those expected for noninteracting or weakly coupled ions for room temperature susceptibilities, consistent with what is found here. Upon decreasing temperature, the χT product for each of the three compounds continuously decreases to reach a minimum value at 1.8 K.

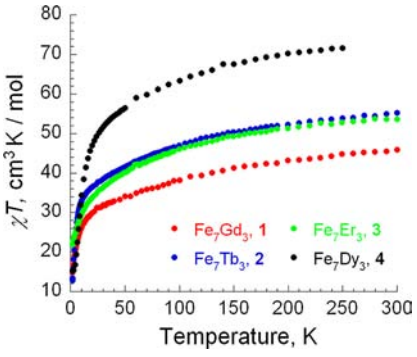

Figure 2. Temperature dependence of the χT products for compounds **1**−**4** at 0.1 T.

Table 2. Comparison of dc Magnetic Data for Compounds 1−4

	1 (Gd)	**2** (Tb)	**3** (Er)	**4** (Dy)[10l]
ground-state term of Ln^{III} ion	$^8S_{7/2}$	$^7F_6$	$^4I_{15/2}$	$^6H_{15/2}$
g for Ln^{III} ion	2	$^3/_2$	$^6/_5$	$^4/_3$
C (cm^3K mol^{-1}) per Ln^{III} ion[4b]	7.87	11.82	11.50	14.17
χT (cm^3K mol^{-1}) expected value for Ln_3Fe_7 at RT	54.25	66.08	65.12	73.14
χT (cm^3K mol^{-1}) experimental value for Ln_3Fe_7 at RT	45.8	55.4	53.3	71.6
χT (cm^3K mol^{-1}) experimental value for Ln_3Fe_7 at 1.8 K	14.8	12.8	21.9	15.4
magnetization (μ_B) observed at 7 T and 1.8 K (or 2 K)	28.1	19.6	22.5	24.6
Curie constant (cm^3 K mol^{-1}) above 100 K	44.3	54.7	56.8	72.8
Weiss constant, θ (K), above 100 K	−20.5	−19.4	−25.1	−24.0

Given that Gd^{III} is essentially an isotropic ion without orbital contributions to the ground state, the monotonic decrease of the χT versus T plot for **1**, with no hint of an upturn at even the lowest temperatures, suggests that the interactions between the Fe^{III} and Gd^{III} ions should be mainly antiferromagnetic. This might also be the case for the analogues **2** and **3**, but for these compounds, the thermal behavior of χT will be additionally complicated by depopulation of the Stark sublevels of the anisotropic Tb^{III} and Er^{III} ions, which can also contribute to the decrease of χT.[4a,23] A fit of the experimental data to a Curie−Weiss law between 100 and 300 K gives sets of Curie and Weiss constants that are listed in Table 2. The obtained Curie constants are all consistent with the experimental room temperature χT values, and the negative Weiss constants confirm the presence of dominating antiferromagnetic interactions between the spin carriers.

The field dependences of the magnetization of compounds **1**−**3** at low temperatures show that in all cases the magnetization smoothly increases with the applied dc field (Figure S2 in the SI) with no clear saturation even at 7 T and reaches the values given in Table 2. Moreover, the reduced magnetization curves are not superposed onto a single master curve. This behavior indicates the presence of magnetic anisotropy as well as the possible population of low-lying excited states. For the Gd^{III} compound **1**, the magnetization only reaches 28.1 μ_B at 7 T, which is much smaller than the predicted 56 μ_B if the magnetic field were to overcome the antiferromagnetic interactions and align all of the spins parallel.

Considering the structure, the seven iron centers form two Gd_2Fe_2 moieties and one $GdFe_3$ chain, with these two sorts of structural motif linked only through the gadolinium centers (Figure 1). Within each of these, the Fe^{III} ions will be antiferromagnetically coupled, giving net spins of $S = 0$ (Fe_2) and $S = {}^5/_2$ (Fe_3) at low temperatures. The observed magnetization for **1** at 7 T is only slightly higher than the value predicted, 26 μ_B, for three Gd^{III} ions with spins parallel and the contributions from the Fe_2 and Fe_3 units. This indicates that the applied magnetic fields up to 7 T can easily overcome any antiferromagnetic Gd−Gd and Gd−Fe interactions but that a field of 7 T can only begin to overcome the much stronger Fe−Fe interactions. In the case of the Er^{III} analogue **3**, following the initial rapid increase of the magnetization at 2 K, there is a hint of a step at 14 μ_B and 2.5 T (Figure S3 in the SI), beyond which the

dx.doi.org/10.1021/ic401011d | *Inorg. Chem.* 2013, 52, 11767−11777

rate of increase of the magnetization increases again. A similar but better defined step was also observed for the dysprosium analogue **4**.[10l]

For compounds **2** and **3**, the presence of anisotropy in these compounds will contribute to the lack of saturation of the magnetization. Because **4** was found to show SMM behavior with a high thermal barrier,[10l] ac susceptibility measurements were carried out under zero dc field for compounds **1**−**3**. No out-of-phase signal was found above 1.8 K for **1** and **3**, but for the Tb^{III} compound **2**, a clear out-of-phase signal (about 15% of the in-phase signal) was observed below 3 K, indicating slow relaxation of the magnetization (Figure 3). Both the in-phase and out-of-

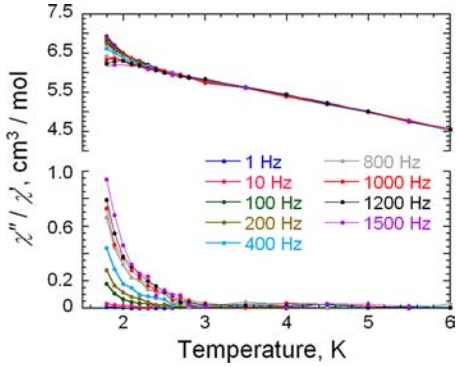

Figure 3. Temperature dependence of the in-phase (top) and out-of-phase (bottom) components of the ac magnetic susceptibility for **2** under zero dc field.

phase signals are frequency-dependent, indicating that this compound exhibits slow relaxation and might be a SMM. However, the χ'' signal showed no maximum above 1.8 K, suggesting that the barrier to relaxation is less than U_{eff} = 33.4 K found for **4**.[10l] Furthermore, because ac susceptibility measurements under a small dc field resulted in no significant change to the relaxation rate (Figure S4 in the SI), we can conjecture that, as found for **4**,[10l] there is no significant quantum tunneling of the magnetization at or above 1.8 K.

3.4. Mössbauer Spectral Studies. The Mössbauer spectra of **1**−**4**, obtained at 295 or 283 K, are shown in Figure 4, and those obtained at 3 K are shown in Figure 5. The complete sets of temperature-dependent Mössbauer spectra for **1**−**3** are shown in Figures S5−S7 in the SI. The spectra of **4**, which were reported previously,[10l] are included in Figures 4 and 5 for comparison.

The spectra of **1**−**3** at temperatures at and above 20, 55, and 40 K, respectively, are fully consistent with the presence of seven paramagnetic high-spin Fe^{III} sites and indicate the absence of any long-range magnetic order or the onset of any slow paramagnetic relaxation. In contrast, at 10, 40, and 40 K, respectively, the Mössbauer spectra of **1**−**3** reveal clear evidence that some of the Fe^{III} sites are beginning to exhibit slow paramagnetic relaxation on the Mössbauer time scale.

As was the case for **4**, the molecular structures of **1**−**3** show the presence of one five-coordinate Fe^{III} site and six pseudooctahedral Fe^{III} sites, the latter of which all have very similar average Fe−O bond distances but rather different distortions from an octahedral coordination environment.[10l] Hence, as is shown in Figure 4, the paramagnetic spectra of **1**−**4** observed at the higher temperatures were fitted as the superposition of six symmetric Lorentzian quadrupole doublets with the same line width and with relative areas of *x*:2:1:1:1:1 and assigned to the seven crystallographically inequivalent Fe^{III} sites. We note that two of

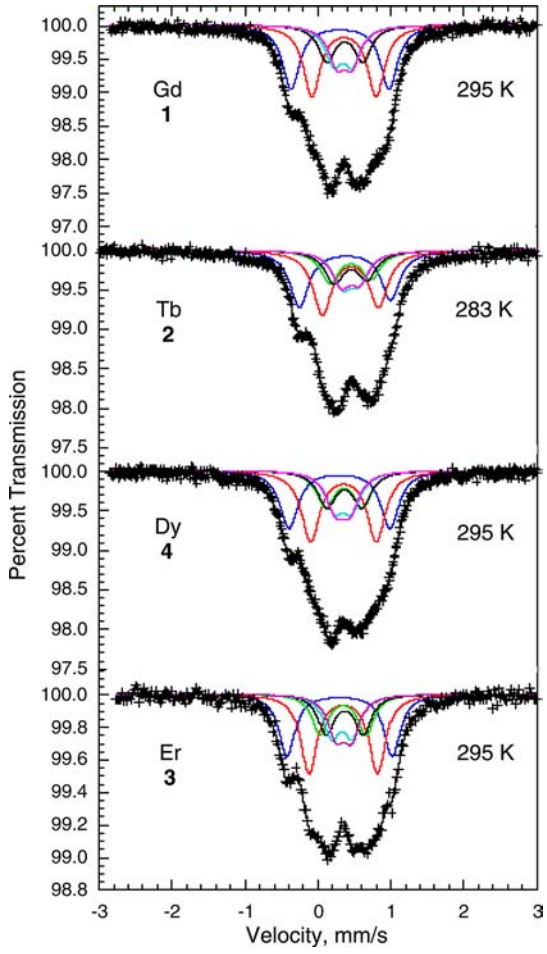

Figure 4. Mössbauer spectra of **1**−**4** obtained at 283 or 295 K. The blue quadrupole doublets are assigned to the Fe(1) five-coordinate Fe^{III} site, and the remaining five doublets are assigned to the Fe(2)−Fe(7) pseudooctahedral Fe^{III} sites. The spectrum of **4** was taken from ref 10l.

these have essentially equivalent Mössbauer spectral parameters. These fits involved adjustment of the parameters for six isomer shifts, six quadrupole splittings, one line width, and the total spectral area. Preliminary fits, in which the relative area of *x* was normalized to unity, led to a systematic misfit at ca. −0.4 mm s^{-1}, as indicated by the lack of calculated intensity on the left side of the absorption profile. Hence, the relative area, *x*, of the first component was adjusted and found to have a value greater than 1. All of these fits have χ^2 values very close to unity and are shown as solid black lines in Figures 4 and S5−S7 in the SI. This is the same model that we used earlier[10l] to fit the spectra of **4**, and further details about the site assignments can be found in this reference. The temperature dependence of the isomer shift and quadrupole splitting of five-coordinate Fe(1) and the weighted-average isomer shift and quadrupole splitting of six-coordinate Fe(2)−Fe(7) are shown in Figure 6, and the resulting parameters are given in Tables S1−S3 in the SI. The five-coordinate Fe(1) isomer shift is ca. 0.08 mm s^{-1} smaller than the six-coordinate Fe(2)−Fe(7) isomer shifts, in very good agreement with the empirical rule stating that the isomer shift decreases by 0.1 mm s^{-1} for a decrease of 1 in the coordination number.[24,25]

Although a specific assignment of the pseudooctahedral Fe(2)−Fe(7) sites, based on the relative distortions of the coordination environments, is not absolutely certain, tentative assignments as previously made[10l] were used for **1**−**3**. The

dx.doi.org/10.1021/ic401011d | *Inorg. Chem.* 2013, 52, 11767−11777

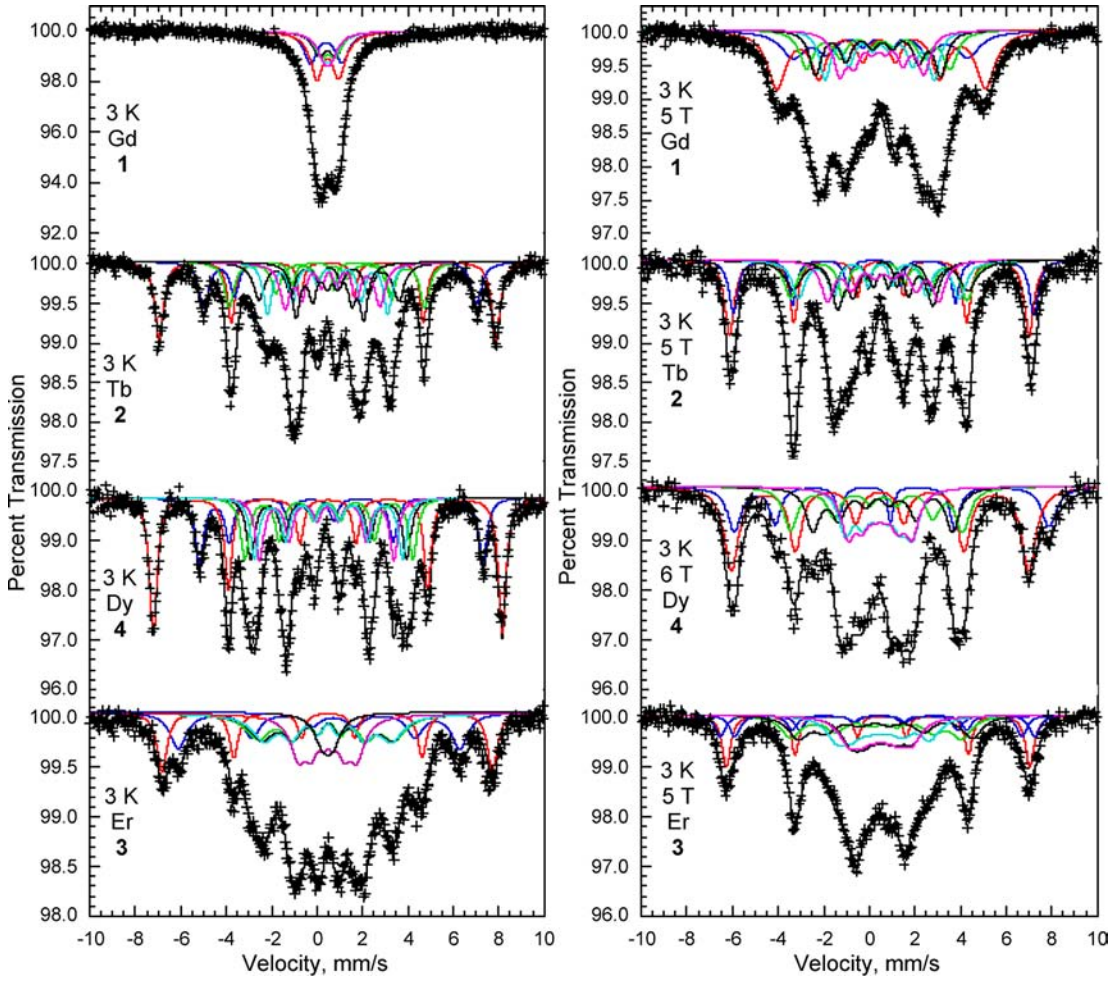

Figure 5. Mössbauer spectra of **1**−**4** obtained at 3 K, left, and at 3 K in an applied field of 5 or 6 T, right. The blue components are assigned to the Fe(1) five-coordinate Fe^{III} site, and the remaining components are assigned to the Fe(2)−Fe(7) pseudooctahedral Fe^{III} sites. The spectra of **4** were taken from ref 10l.

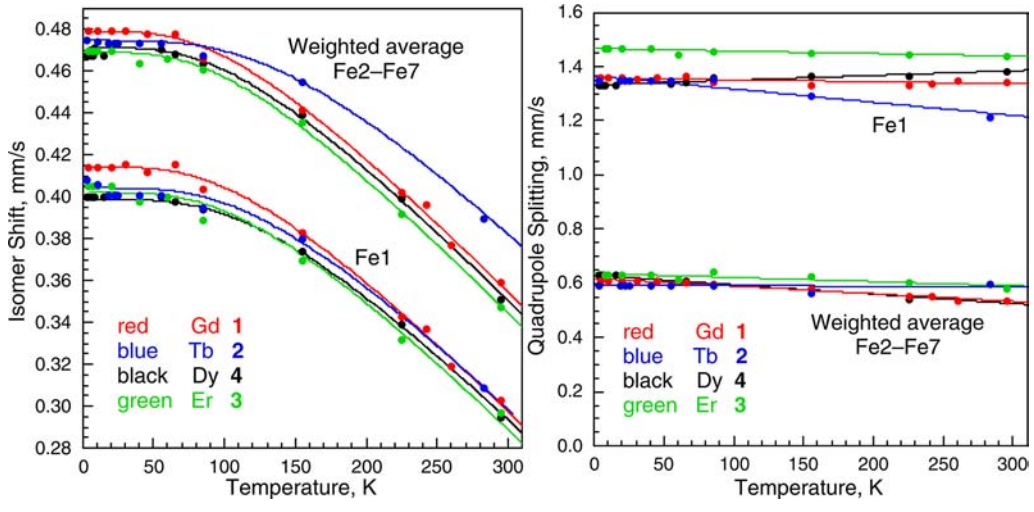

Figure 6. Temperature dependence of the isomer shifts, left, and quadrupole splittings, right, for Fe(1) and the weighted-average values for the Fe(2)−Fe(7) Fe^{III} sites observed for **1**−**4** shown in red, blue, green, and black, respectively. For the isomer shifts, the solid lines are the results of fits with the Debye model for the second-order Doppler shift. The data for **4** were obtained from ref 10l.

paramagnetic quadrupole splittings are essentially independent of \ temperature as expected for high-spin Fe^{III} ions for which the quadrupolar interaction originates only from a lattice contribution to the electric-field gradient.

The solid lines in the left portion of Figure 6 result from fits with the Debye model for the second-order Doppler shift, and the resulting Mössbauer temperatures, Θ_M, are 490(23), 552(21), 490(23), and 541(12) K for the Fe(1) site and

dx.doi.org/10.1021/ic401011d | *Inorg. Chem.* 2013, 52, 11767−11777

421(11), 621(10), 424(19), and 445(11) K for the Fe(2)−Fe(7) sites in **1**−**4**, respectively. Except for the case of compound **2**, the Mössbauer temperature for Fe(1) is larger than that for the other six iron sites because the Fe(1) ion is more tightly bound in its 5-fold coordination site than are the remaining six pseudooctahedral Fe^{III} ions. It is not clear why the 621(10) K value is so large for **2**. The temperature dependences of the logarithm of the Mössbauer spectral absorption areas observed for **1**−**4** are shown in Figure S8 in the SI along with the fits using the Debye model for a solid. The solid lines corresponding to Mössbauer-effect-derived Debye temperatures, Θ_D, of 140(2), 136(3), 141(2), and 137(2) K for **1**−**4**, respectively, indicate that, as expected, the four compounds have the same Θ_D value within experimental error. As is usually observed, the Θ_M temperatures are larger than the Θ_D temperatures because the isomer shift is more sensitive to high-frequency phonons than the absorption area.[26,27]

A preliminary fit of the 10 K Mössbauer spectrum of **1** with the six doublets used at 20 K revealed a distinct broadening of each of the quadrupole doublet line widths from 0.285 mm s^{-1} at 20 K to 0.410 mm s^{-1} at 10 K. This broadening indicates the onset of slow magnetic relaxation upon cooling below 20 K on the Mössbauer time scale. Hence, the Mössbauer spectra of **1** at 3, 4.2, 10, and 20 K were fitted with a relaxation profile that used the Dattagupta and Blume[28] formalism. This relaxation profile is the sum of six relaxation-broadened components that all experience the same temperature-independent hyperfine field of 35 T and the same relaxation frequency. The hyperfine field is assumed to relax between the six $\pm x$, $\pm y$, and $\pm z$ directions, representing an isotropic relaxation in agreement with the isotropic Gd^{III} magnetic moment. The intrinsic line width was constrained to 0.275 mm s^{-1}, the observed line width at 45 K (see Table S3 in the SI). The value of the hyperfine field was constrained to 35 T in view of the hyperfine fields observed under an applied field of 5 T (see the right portion of Figure 5), and this value was used as an average hyperfine field for all six components. The six isomer shifts and quadrupole splittings were constrained to values in agreement with those observed at and above 30 K. Specifically, the isomer shifts were constrained to 0.416, 0.484, 0.498, 0.466, 0.470, and 0.476 mm s^{-1}, and the quadrupole splittings were constrained to 1.356, 0.938, 0.544, 0.672, 0.334, and 0.224 mm s^{-1} for Fe1, Fe3 and Fe5, Fe2, Fe4, Fe7, and Fe6, respectively, in agreement with the assignment proposed[10l] earlier. The resulting fits are shown in Figure S5 in the SI. The relaxation frequency increases from 860 (20) MHz at 3 K to 35000 (5000) MHz at 20 K, as expected for a thermally activated relaxation process.

In contrast to the magnetic behavior of **1**, the behavior of **2** and **3** is quite different, as may be seen in the left portion of Figure 5. At 3 K, the Mössbauer spectrum of **2**, which resembles[10l] that of **4**, clearly reveals well-defined effective hyperfine fields because their relaxation time is much longer than the Larmor precession period. Furthermore, at 3 K the spectrum of **3** is different again in that it exhibits sextets with spectral line widths that are much broader and suggests that the relaxation time of the hyperfine fields in **3** is smaller than those in **2** and **4**. In view of the similarity of the structures of the four compounds, these differences must result, at least to a large extent, from the differing electronic properties of the lanthanide ions (see Table 2). The observation of sextets in the Mössbauer spectra, resulting from a relaxation time longer than the Larmor precession time of 5×10^{-8} s, suggests that different preexponential factors, τ_0, in the different Ln_3Fe_7 coordination clusters may also contribute to the difference in the spectra observed at 3 K.

Detailed analysis of the 3 K Mössbauer spectra of **2** and **3** is somewhat difficult but is facilitated, in part, by the presence of larger effective hyperfine fields on two or more of the Fe^{III} sites. This is best observed as the presence of the outer two lines at both positive and negative velocities in the spectra of **2** and **3** (Figure 5), which was also observed[10l] earlier in **4**. In fitting the Mössbauer spectra of **2** and **3**, the isomer shifts and quadrupole splittings of the individual Fe^{III} sites were constrained to be the same as those observed in the lowest-temperature paramagnetic spectra (see Tables S1−S3 in the SI), and only the angle θ between the effective hyperfine field and the principal axis of the electric-field gradient at each site has been fitted. In agreement with the earlier fits[10l] of **4**, the sextet with the second-largest field in **2** and **3**, the blue sextet in Figure 5 was found to have parameters that were consistent with the five-coordinate Fe(1) site. Furthermore, the line widths and relative areas of the outer two sextets were fit but with the remaining sextets constrained to have the same line widths and relative areas. A very similar approach was used in the analysis of the low-temperature spectra of **4**, and more details of these fits have been reported earlier.[10l]

One of the unusual features of the 3 K spectra of **2**−**4** is the different relative areas observed (Figure 5) for the two outer sextets. The ratios of the relative areas at 3 K are 1.50:1 for **2**, 1.00:1 for **3**, and 1.90:1 for **4**. In the latter case, the 1.90:1 ratio, rather than 2:1, is a consequence of the larger recoil-free fraction of the five-coordinate Fe(1) site and the structural similarity[10l] of the Fe(3) and Fe(5) six-coordinate Fe^{III} sites in **4**. It was found that the outer two sextets observed for **2** could *not* be fit with a ratio close to 1:1 or 2:1. Clearly, small structural differences in the clusters in **1**−**4** must lead to differing magnetic site degeneracies for the outer two sextets, and these differences lead to differing relative areas.

As indicated by the observed broadening in Figures S6 and S7 in the SI, the Mössbauer spectra of **2** and **3** show the onset of slow paramagnetic relaxation at and below 40 and 15 K, respectively. Ideally, one would like to be able to model this broadening in a fashion similar to that used above for **1**. Unfortunately, in the presence of the anisotropy of the Tb^{III} and Er^{III} ions and of seven crystallographically inequivalent Fe^{III} sites exhibiting very different hyperfine fields, it was not possible to simulate the spectra with a relaxation profile. Hence, to fit the broadening of the spectra, a broad component was added to the fit and is shown as the black component at 40, 25, 22, and 18 K in Figure S6 in the SI and at 15, 10, and 7 K in Figure S7 in the SI.

As can be seen in the right portion of Figure 5 and in Figures S9−S11 in the SI, the response of **1**−**4** to a transverse applied magnetic field is rather different. In each case, the spectral profile first broadens at small-to-moderate applied fields and then sharpens at large applied fields. A complete description of this behavior is very difficult because of the complexity of the spectra, the polycrystalline nature of the absorbers, and the effect of the applied field both on the hyperfine magnetic states of the lanthanide ion and their interactions with the iron ions and on the direct relaxation process of the magnetization, whose frequency[29] is proportional to the square of the applied field. However, at 3 K in an applied field of 5 or 6 T, the outer sextets observed for **2**−**4** and shown in red and blue in the figures are actually somewhat simplified. Indeed, it appears that in all three compounds the effective hyperfine field of the red sextet, the sextet with the largest effective hyperfine field in the absence of an applied field, is reduced between a 0 and 5 T applied field by 5.2(2) T for **2** and 4.0(2) T for **3**, as compared with the reduction between a 0 and 6 T applied field of 7.3(2) T for **4**. Thus, it

dx.doi.org/10.1021/ic401011d | *Inorg. Chem.* 2013, 52, 11767−11777

appears that in each compound the applied field subtracts from the effective hyperfine field and there is no apparent splitting of this sextet.

In contrast, the response to an applied field is very different for the blue sextet, which is the sextet with the second-largest effective hyperfine field and assigned to the five-coordinate Fe(1) site. In **2**, the effective field of this sextet increases by 3.0(2) T in an applied field of 5 T. In stark contrast, in **3**, this sextet is split such that the effective field of half of it remains virtually unchanged and the other half increases by 3.9(2) T in an applied field of 5 T. For comparison, in **4**, the effective hyperfine field of this sextet increases by 3.0(2) T in an applied field of 6 T, and there is no indication of any splitting of this sextet.

4. CONCLUSIONS

The reaction of $mdeaH_2$ and benzoic acid with $FeCl_3$ and $LnCl_3$ or $Ln(NO_3)_3$ yields a series of decanuclear coordination clusters, $[Ln_3Fe_7(\mu_4\text{-}O)_2(\mu_3\text{-}OH)_2(mdea)_7(\mu\text{-benzoate})_4(N_3)_6]\cdot x$Solv, where Ln = Gd^{III} (**1**), Tb^{III} (**2**), and Er^{III} (**3**). The structures of **1**−**3** have three and seven crystallographically distinct Ln^{III} and Fe^{III} ions; six of the Fe^{III} ions are *pseudo*octahedrally coordinated, whereas the seventh has a trigonal-bipyramidal coordination geometry. Macroscopic dc and ac magnetic susceptibility studies indicate that intracluster antiferromagnetic interactions between the Ln^{III} and Fe^{III} ions in **1**−**3** are dominant and yield a ferrimagnetic arrangement of spin carriers. ac χ' and χ'' susceptibility studies reveal that **2** undergoes a slow relaxation of its magnetization.

The Mössbauer spectra of **1**−**3** obtained between 55 and 295 K are characteristic of paramagnetic behavior and exhibit six partially resolved Fe^{III} quadrupole doublets, in the ratio of *x*:2:1:1:1:1, that may be assigned to the trigonal-bipyramidal Fe(1) site, the *pseudo*octahedral Fe(3) and Fe(5) sites, and the four remaining *pseudo*octahedral sites.

Because of their different time windows, ^{57}Fe Mössbauer spectroscopy and ac magnetic susceptibility measurements provide an apparently different view of the SMM dynamics in the four Ln_3Fe_7 coordination clusters. Specifically, the time window for ^{57}Fe Mössbauer spectroscopy is the period of the Larmor precession of the ^{57}Fe nuclear magnetic moment around the magnetic hyperfine field, whereas the time window for ac magnetic susceptibility measurements is typically given by the period of the ac field. The Larmor precession period is inversely proportional to the ^{57}Fe nuclear magnetic moment and the hyperfine field and varies between 8.4×10^{-8} and 1.7×10^{-8} s for a hyperfine field between 10 and 50 T, respectively. In the present ac magnetic susceptibility measurements, the ac field period varies between 6×10^{-4} and 1 s.

At 3 K, the ^{57}Fe Mössbauer spectra of all four clusters show at least the onset of slow magnetic relaxation; i.e., at least some broadening or sextets, resulting from the slow precession of the ^{57}Fe nuclear moment around the magnetic hyperfine field, are observed (see the left portion of Figure 5). In **4**, because well-developed sharp sextets are observed for all seven Fe^{III} sites, the precession period of all hyperfine fields is greater than the longest 3 K Larmor precession period of 4.6×10^{-8} s.[10l] From the Arrhenius fit[10l] of the ac magnetic susceptibility measurements, $\tau = \tau_0 \exp(U_{eff}/kT)$, with $\tau_0 = 6.6 \times 10^{-8}$ s and U_{eff} = 33.4 K, a relaxation time of 4.5×10^{-3} s is obtained at 3 K and is indeed much greater than 4.6×10^{-8} s.

Because in clusters **1**−**3** the magnetic relaxation is faster than in **4**, only a more limited description can be proposed. In **2**, the 3 K ^{57}Fe Mössbauer spectrum exhibits well-developed sextets but broader sextets than those observed in **4** (see Figure 5). Similarly, the ac magnetic susceptibility measurements (see Figure 3) show the onset of slow magnetic relaxation below 3 K, but in contrast to the observation for **4**, no maximum in the temperature dependence of the out-of-phase susceptibility was observed. Hence, both techniques indicate that the relaxation time in **2** is shorter than in **4**.

In **3**, the 3 K ^{57}Fe Mössbauer spectrum exhibits broad sextets (see Figure 5), indicating a relaxation time comparable with an average Larmor precession period of 3.8×10^{-8} s, in agreement with the absence of any slow relaxation in the ac magnetic measurements.

Finally, in **1**, the 3 K ^{57}Fe Mössbauer spectrum (see Figure S9 in the SI) exhibits only a small amount of broadening that has been modeled with a relaxation profile, indicating a relaxation time of $0.116(3) \times 10^{-8}$ s, which is, of course, much too small to be probed by ac susceptibility measurements.

In the Ln_3Fe_7 clusters, the influence of the magnetic lanthanide ions on the Fe_7 subcluster is well illustrated in the 3−10 K Mössbauer spectra. Only compounds **2**−**4** show a significant slowing of the spin relaxation of all iron sites in the form of at least resolved broadened or sharp sextets in the absence of an applied magnetic field. The reason for this behavior lies in the large and specific anisotropy of the Tb^{III}, Dy^{III}, and Er^{III} ions, in contrast to the isotropic character of the Gd^{III} ion. In addition, the spectra for all compounds measured at 3 K with increasing applied field show changes in the internal magnetic field values, consistent with the effect of the local spin polarization along the applied magnetic field direction, which may be taken as the Mössbauer signature of an antiparallel-spin-coupled iron molecular paramagnet.

■ ASSOCIATED CONTENT

Supporting Information

Frequency dependence of the in-phase, χ', and out-of-phase, χ'', components of the ac magnetic susceptibility obtained for **2** at different dc fields, field dependence of magnetization, selected Mössbauer spectra, and CIF files for the crystal structures of **1** and **3**. This material is available free of charge via the Internet at http://pubs.acs.org.

■ AUTHOR INFORMATION

Corresponding Authors

*E-mail: glong@mst.edu.
*E-mail: annie.powell@kit.edu.

Present Address

‡Interdisciplinary Research Centre in Biomedical Materials, COMSATS Institute of Information Technology, Lahore, Pakistan.

Notes

The authors declare no competing financial interest.

■ ACKNOWLEDGMENTS

The authors acknowledge with thanks financial support of the DFG (Center for Functional Nanostructures) and Fonds National de la Recherche Scientifique, Belgium (Grants 9.456595 and 1.5.064.05) as well as the Synchrotron Light Source ANKA for the provision of instruments at the SCD beamline. We thank Dr. O. Presly (Oxford Diffraction) for measuring the dataset for the structure of **3**.

REFERENCES

(1) (a) Sessoli, R.; Tsai, H.-L.; Schake, A. R.; Wang, S.; Vincent, J. B.; Folting, K.; Gatteschi, D.; Christou, G.; Hendrickson, D. N. *J. Am. Chem. Soc.* **1993**, *115*, 1804−1816. (b) Christou, G.; Gatteschi, D.; Hendrickson, D. N.; Sessoli, R. *MRS Bull.* **2000**, *25*, 66−67. (c) Aromi, G.; Aubin, S. M. J.; Bolcar, M. A.; Christou, G.; Eppley, H. J.; Folting, K.; Hendrickson, D. N.; Huffman, J. C.; Squire, R. C.; Tsai, H.-L.; Wang, S.; Wemple, M. W. *Polyhedron* **1998**, *17*, 3005−3020. (d) Christou, G. *Polyhedron* **2005**, *24*, 2065−2075.

(2) (a) Sessoli, R.; Gatteschi, D.; Caneschi, A.; Novak, M. A. *Nature* **1993**, *365*, 141−143. (b) Thomas, L.; Lionti, L.; Ballou, R.; Gatteschi, D.; Sessoli, R.; Barbara, B. *Nature* **1996**, *383*, 145−147.

(3) (a) Kong, X.-J.; Ren, Y.-P.; Chen, W.-X.; Long, L.-S.; Zheng, Z.; Huang, R.-B.; Zheng, L.-S. *Angew. Chem., Int. Ed.* **2008**, *47*, 2398−2401. (b) Xu, Z.; Read, P. W.; Hibbs, D. E.; Hursthouse, M. B.; Abdul Malik, K. M.; Patrick, B. O.; Rettig, S. J.; Seid, M.; Summers, D. A.; Pink, M.; Thompson, R. C.; Orvig, C. *Inorg. Chem.* **2000**, *39*, 508−516. (c) Zaleski, C. M.; Depperman, E. C.; Kampf, J. W.; Kirk, M. L.; Pecoraro, V. L. *Angew. Chem., Int. Ed.* **2004**, *43*, 3912−3914. (d) Ishikawa, N. *Polyhedron* **2007**, *26*, 2147−2153. (e) Xiang, S.; Hu, S.; Sheng, T.; Fu, R.; Wu, X.; Zhang, X. *J. Am. Chem. Soc.* **2007**, *129*, 15144−15146. (f) Lescouezec, R.; Toma, L. M.; Vaissermann, J.; Verdaguer, M.; Delgado, F. S.; Ruiz-Perez, C.; Lloret, F.; Julve, M. *Coord. Chem. Rev.* **2005**, *249*, 2691−2729. (g) Coulon, C.; Miyasaka, H.; Clérac, R. *Struct. Bonding (Berlin)* **2006**, *122*, 163−206. (h) Liu, T.; Fu, D.; Gao, S.; Zhang, Y.; Sun, H.; Su, G.; Liu, Y. *J. Am. Chem. Soc.* **2003**, *125*, 13976−13977.

(4) (a) Sorace, L.; Benelli, C.; Gatteschi, D. *Chem. Soc. Rev.* **2011**, *40*, 3092−3104. (b) Benelli, C.; Gatteschi, D. *Chem. Rev.* **2002**, *102*, 2369−2388. (c) Güdel, H. U.; Furrer, A.; Blank, H. *Inorg. Chem.* **1990**, *29*, 4081−4084.

(5) Bencini, A.; Benelli, C.; Caneschi, A.; Carlin, R. L.; Dei, A.; Gatteschi, D. *J. Am. Chem. Soc.* **1985**, *107*, 8128−8136.

(6) (a) Costes, J.-P.; Clemente-Juan, J.-M.; Dahan, F.; Milon, J. *Inorg. Chem.* **2004**, *43*, 8200−8202. (b) Osa, S.; Kido, T.; Matsumoto, N.; Re, N.; Pochaba, A.; Mrozinski, J. *J. Am. Chem. Soc.* **2004**, *126*, 420−421. (c) Zhang, M.-B.; Zhang, J.; Zheng, S.-T.; Yang, G.-Y. *Angew. Chem.* **2005**, *117*, 1409−1412. (d) Zhang, J.-J.; Hu, S.-M.; Xiang, S.-C.; Sheng, T.; Wu, X.-T.; Li, Y.-M. *Inorg. Chem.* **2006**, *45*, 7173−7181. (e) Mori, F.; Nyui, T.; Ishida, T.; Nogami, T.; Choi, K.-Y.; Nojiri, H. *J. Am. Chem. Soc.* **2006**, *128*, 1440−1441. (f) Aronica, C.; Pilet, G.; Chastanet, G.; Wernsdorfer, W.; Jacquot, J.-F.; Luneau, D. *Angew. Chem., Int. Ed.* **2006**, *45*, 4659−4662. (g) Novitchi, G.; Costes, J.-P.; Tuchagues, J.-P.; Vendier, L.; Wernsdorfer, W. *New J. Chem.* **2008**, *32*, 197−200. (h) Novitchi, G.; Wernsdorfer, W.; Chibotaru, L.; Costes, J.-P.; Anson, C. E.; Powell, A. K. *Angew. Chem., Int. Ed.* **2009**, *48*, 1614−1619.

(7) (a) Benelli, C.; Murrie, M.; Parsons, S.; Winpenny, R. E. P. *J. Chem. Soc., Dalton Trans.* **1999**, 4125−4126. (b) Zaleski, C.; Depperman, E.; Kampf, J.; Kirk, M.; Pecoraro, V. *Angew. Chem., Int. Ed.* **2004**, *43*, 3912−3914. (c) Mishra, A.; Wernsdorfer, W.; Abboud, K.; Christou, G. *J. Am. Chem. Soc.* **2004**, *126*, 15648−15648. (d) Mishra, A.; Wernsdorfer, W.; Parsons, S.; Christou, G.; Brechin, E. K. *Chem. Commun.* **2005**, 2086−2088. (e) Mereacre, V.; Ako, A. M.; Clérac, R.; Wernsdorfer, W.; Filoti, G.; Bartolomé, J.; Anson, C. E.; Powell, A. K. *J. Am. Chem. Soc.* **2007**, *129*, 9248−9249. (f) Stamatotos, T. C.; Teat, S. J.; Wernsdorfer, W.; Christou, G. *Angew. Chem., Int. Ed.* **2009**, *48*, 521−524. (g) Ako, A. M.; Mereacre, V.; Clérac, R.; Wernsdorfer, W.; Hewitt, I. J.; Anson, C. E.; Powell, A. K. *Chem. Commun.* **2009**, 544−546. (h) Li, M.; Lan, Y.; Ako, A. M.; Wernsdorfer, W.; Anson, C. E.; Buth, G.; Powell, A. K.; Wang, Z. M.; Gao, S. *Inorg. Chem.* **2010**, *49*, 11587−11594. (i) Papatriantafyllopoulou, C.; Wernsdorfer, W.; Abboud, K. A.; Christou, G. *Inorg. Chem.* **2011**, *50*, 421−423.

(8) (a) Chandrasekhar, V.; Pandian, B. M.; Azhakar, R.; Vittal, J. J.; Clérac, R. *Inorg. Chem.* **2007**, *46*, 5140−5142. (b) Huang, Y. G.; Wang, X. T.; Jiang, F. L.; Gao, S.; Wu, M. Y.; Gao, Q.; Wei, W.; Hong, M. C. *Chem.—Eur. J.* **2008**, *14*, 10340−10347. (c) Yamaguchi, T.; Costes, J.-P.; Kishima, Y.; Kojima, M.; Sunatsuki, Y.; Bréfuel, N.; Tuchagues, J.-P.; Vendier, L.; Wernsdorfer, W. *Inorg. Chem.* **2010**, *49*, 9125−9135.

(9) (a) Brechin, E. K.; Harris, S.; Parsons, S.; Winpenny, R. E. P. *J. Chem. Soc., Dalton Trans.* **1997**, 1665−1666. (b) Costes, J.-P.; Dahan, F.; Dupuis, A.; Laurent, J.-P. *Inorg. Chem.* **1997**, *36*, 4284−4286. (c) Shiga, T.; Ito, N.; Hidaka, A.; Okawa, H.; Kitagawa, S.; Ohba, M. *Inorg. Chem.* **2007**, *46*, 3492−3501. (d) Madalan, A. M.; Avarvari, N.; Fourmigué, M.; Clérac, R.; Chibotaru, L. F.; Clima, S.; Andruh, M. *Inorg. Chem.* **2008**, *47*, 940−950. (e) Efthymiou, C. G.; Stamatatos, T. C.; Papatriantafyllopoulou, C.; Tasiopoulos, A. J.; Wernsdorfer, W.; Perlepes, S. P.; Christou, G. *Inorg. Chem.* **2010**, *49*, 9737−9739.

(10) (a) Ferbinteanu, M.; Kajiwara, T.; Choi, K.-Y.; Nojiri, H.; Nakamoto, A.; Kojima, N.; Cimpoesu, F.; Fujimura, Y.; Takaishi, S.; Yamashita, M. *J. Am. Chem. Soc.* **2006**, *128*, 9008−9009. (b) Murugesu, M.; Mishra, A.; Wernsdorfer, W.; Abboud, K.; Christou, G. *Polyhedron* **2006**, *25*, 613−625. (c) Pointillart, F.; Bernot, K.; Sessoli, R.; Gatteschi, D. *Chem.—Eur. J.* **2007**, *13*, 1602−1609. (d) Costes, J. P.; Dupuis, A.; Laurent, J. P. *Eur. J. Inorg. Chem.* **1998**, 1543−1546. (e) Costes, J. P.; Dahan, F.; Dumestre, F.; Clemente-Juan, J. M.; Garcia-Tojal, J.; Tuchagues, J. P. *Dalton Trans.* **2003**, 464−468. (f) Turta, C. I.; Prodius, D. N.; Mereacre, V. M.; Shova, S. G.; Gdaniec, M.; Simonov, Yu. A.; Kuncser, V.; Filoti, G.; Caneschi, A.; Sorace, L. *Inorg. Chem. Commun.* **2004**, *7*, 576−578. (g) Figuerola, A.; Ribas, J.; Llunell, M.; Casanova, D.; Maestro, M.; Alvarez, S.; Diaz, C. *Inorg. Chem.* **2005**, *44*, 6939−6948. (h) Ako, A. M.; Mereacre, V.; Clérac, R.; Hewitt, I. J.; Lan, Y.; Anson, C. E.; Powell, A. K. *Dalton Trans.* **2007**, 5245−5247. (i) Mukherjee, S.; Lan, Y.; Novitchi, G.; Kostakis, G.; Anson, C. E.; Powell, A. K. *Polyhedron* **2009**, *28*, 1782−1787. (j) Bartolomé, J.; Filoti, G.; Kuncser, V.; Schinteie, G.; Mereacre, V.; Anson, C. E.; Powell, A. K.; Prodius, D.; Turta, C. *Phys. Rev. B* **2009**, *80* (014430), 1−16. (k) Akhtar, M. N.; Mereacre, V.; Novitchi, G.; Tuchagues, J.-P.; Anson, C. E.; Powell, A. K. *Chem.—Eur. J.* **2009**, *15*, 7278−7282. (l) Abbas, G.; Lan, Y.; Mereacre, V.; Wernsdorfer, W.; Clérac, R.; Buth, G.; Sougrati, M. T.; Grandjean, F.; Long, G. J.; Anson, C. E.; Powell, A. K. *Inorg. Chem.* **2009**, *48*, 9345−9355. (m) Schray, D.; Abbas, G.; Lan, Y.; Mereacre, V.; Sundt, A.; Dreiser, J.; Waldmann, O.; Kostakis, G. E.; Anson, C. E.; Powell, A. K. *Angew. Chem., Int. Ed.* **2010**, *49*, 5185−5188. (n) Zeng, Y.-F.; Xu, G.-C.; Hu, X.; Chen, Z.; Bu, X.-H.; Gao, S.; Sañudo, E. C. *Inorg. Chem.* **2010**, *49*, 9734−9736. (o) Mereacre, V.; Prodius, D.; Lan, Y.; Turta, C.; Anson, C. E.; Powell, A. K. *Chem.—Eur. J.* **2011**, *17*, 123−128. (p) Baniodeh, A.; Hewitt, I. J.; Mereacre, V.; Lan, Y.; Novitchi, G.; Anson, C. E.; Powell, A. K. *Dalton Trans.* **2011**, *40*, 4080−4086. (q) Mereacre, V.; Baniodeh, A.; Anson, C. E.; Powell, A. K. *J. Am. Chem. Soc.* **2011**, *133*, 15335−15337. (r) Mereacre, V. *Angew. Chem., Int. Ed.* **2012**, *51*, 9922−9925. (s) Xiang, H.; Mereacre, V.; Lan, Y.; Lu, T.-B.; Anson, C. E.; Powell, A. K. *Chem. Commun.* **2013**, *49*, 7385−7387.

(11) (a) Rumberger, E. M.; Shah, S. J.; Beedle, C. C.; Zakharov, L. N.; Rheingold, A. L.; Hendrickson, D. N. *Inorg. Chem.* **2005**, *44*, 2742−2752. (b) Murugesu, M.; Habrych, M.; Wernsdorfer, W.; Abboud, K. A.; Christou, G. *J. Am. Chem. Soc.* **2004**, *126*, 4766−4767. (c) Boskovic, C.; Wernsdorfer, W.; Folting, K.; Huffmann, J. C.; Hendrickson, D. N.; Christou, G. *Inorg. Chem.* **2002**, *41*, 5107−5118. (d) Glaser, T.; Liratzis, I.; Lügger, T.; Fröhlich, R. *Eur. J. Inorg. Chem.* **2004**, 2683−2689. (e) Yang, C. I.; Lee, G. H.; Wur, C. S.; Lin, J. G.; Tsai, H. L. *Polyhedron* **2005**, *24*, 2215−2221. (f) Saalfrank, R. W.; Nakajima, T.; Mooren, N.; Scheurer, A.; Maid, H.; Hampel, F.; Trieflinger, C.; Daub, J. *Eur. J. Inorg. Chem.* **2005**, 1149−1153.

(12) (a) Saalfrank, R. W.; Scheurer, A.; Prakash, R.; Heinemann, F. W.; Nakajima, T.; Hampel, F.; Leppin, R.; Pilawa, B.; Rupp, H.; Müller, P. *Inorg. Chem.* **2007**, *46*, 1586−1592. (b) Manoli, M.; Prescimone, A.; Bagai, R.; Mishra, A.; Murugesu, M.; Parsons, S.; Wernsdorfer, W.; Christou, G.; Brechin, E. K. *Inorg. Chem.* **2007**, *46*, 6968−6979. (c) Rajaraman, G.; Murugesu, M.; Sanudo, E. C.; Soler, M.; Wernsdorfer, W.; Helliwell, M.; Muryn, C.; Raftery, J.; Teat, S. J.; Christou, G.; Brechin, E. K. *J. Am. Chem. Soc.* **2004**, *126*, 15445−15457. (d) Foguet-Albiol, D.; Abboud, K.; Christou, G. *Chem. Commun.* **2005**, 4282−4284. (e) Saalfrank, R. W.; Deutscher, Ch.; Sperner, S.; Nakajima, T.; Ako, A. M.; Uller, E.; Hampel, F.; Heinemann, F. W. *Inorg. Chem.* **2004**, *43*, 4372−4382. (f) Saalfrank, R. W.; Maid, H.; Scheurer, A. *Angew. Chem., Int. Ed.* **2008**, *47*, 8794−8824. (g) Ako, A. M.; Mereacre,

V.; Lan, Y.; Anson, C. E.; Powell, A. K. *Chem.—Eur. J.* **2011**, *17*, 4366−4370.
(13) (a) Mereacre, V.; Ako, A. M.; Clérac, R.; Wernsdorfer, W.; Hewitt, I. J.; Anson, C. E.; Powell, A. K. *Chem.—Eur. J.* **2008**, *14*, 3577−3584. (b) Rinck, J.; Novitchi, G.; Van den Heuvel, W.; Ungur, L.; Lan, Y.; Wernsdorfer, W.; Anson, C. E.; Chibotaru, L. F.; Powell, A. K. *Angew. Chem., Int. Ed.* **2010**, *49*, 7583−7587.
(14) (a) Wieghardt, K.; Pohl, K.; Jibril, I.; Huttner, G. *Angew. Chem., Int. Ed.* **1984**, *23*, 77−78. (b) Powell, A. K.; Heath, S. L.; Gatteschi, D.; Pardi, L.; Sessoli, R.; Spina, G.; Del Giallo, F.; Pieralli, F. *J. Am. Chem. Soc.* **1995**, *117*, 2491−2502. (c) Accorsi, S.; Barra, A.-L.; Caneschi, A.; Chastanet, G.; Cornia, A.; Fabretti, A. C.; Gatteschi, D.; Mortalò, C.; Olivieri, E.; Parenti, F.; Rosa, P.; Sessoli, R.; Sorace, L.; Wernsdorfer, W.; Zobbi, L. *J. Am. Chem. Soc.* **2006**, *128*, 4742−4755.
(15) Grunert, C. M.; Reiman, S.; Spiering, H.; Kitchen, J. A.; Brooker, S.; Gütlich, P. *Angew. Chem., Int. Ed.* **2008**, *47*, 2997−2999.
(16) Boudalis, A. K.; Sanakis, Y.; Clemente-Juan, J. M.; Donnadieu, B.; Nastopoulos, V.; Mari, A.; Coppel, Y.; Tuchagues, J.-P.; Perlepes, S. P. *Chem.—Eur. J.* **2008**, *14*, 2514−2526.
(17) Gütlich, P.; Link, R.; Trautwein, A. X. *Mössbauer Spectroscopy and Transition Metal Chemistry*; Springer: Berlin, 1978.
(18) Gatteschi, D.; Sessoli, R.; Villain, J. *Molecular Nanomagnets*; Oxford University Press: Oxford, U.K., 2006.
(19) Brennan, S.; Cowan, P. L. *Rev. Sci. Instrum.* **1992**, *63*, 850−853.
(20) Sheldrick, G. M. *Acta Crystallogr.* **2008**, *A64*, 112−122.
(21) (a) Brown, I. D.; Altermatt, D. *Acta Crystallogr.* **1985**, *B41*, 244−247. (b) Liu, W.; Thorp, H. H. *Inorg. Chem.* **1993**, *32*, 4102−4105.
(22) (a) Werner, R.; Ostrovsky, S.; Griesar, K.; Haase, W. *Inorg. Chim. Acta* **2001**, *326*, 78−88. (b) Canada-Vilalta, C.; O'Brien, T. A.; Brechin, E. K.; Pink, M.; Davidson, E. R.; Christou, G. *Inorg. Chem.* **2004**, *43*, 5505−5521. (c) Gorun, S. M.; Lippard, S. J. *Inorg. Chem.* **1991**, *30*, 1625−1630. (d) Weihe, H.; Güdel, H. U. *J. Am. Chem. Soc.* **1997**, *119*, 6539−6543.
(23) Kahn, M. L.; Sutter, J. P.; Golhen, S.; Guionneau, P.; Ouahab, L.; Kahn, O.; Chasseau, D. *J. Am. Chem. Soc.* **2000**, *122*, 3413−3421.
(24) Schünemann, V.; Paulsen, H. In *Applications of Physical Methods to Inorganic and Bioinorganic Chemistry*; Scott, R. A., Lukehart, C. M., Eds.; Wiley: New York, 2007; p 243.
(25) Zueva, E. M.; Sameera, W. M. C.; Piñero, D. M.; Chakraborty, I.; Devlin, E.; Baran, P.; Lebruskova, K.; Sanakis, Y.; McGrady, J. E.; Raptis, R. G. *Inorg. Chem.* **2011**, *50*, 1021−1029.
(26) Shenoy, G. K.; Wagner, F. E.; Kalvius, G. M. In *Mössbauer Isomer Shifts*; Shenoy, G. K., Wagner, F. E., Eds.; North-Holland: Amsterdam, The Netherlands, 1978; p 49.
(27) Owen, T.; Grandjean, F.; Long, G. J.; Domasevitch, K. V.; Gerasimchuk, N. *Inorg. Chem.* **2008**, *47*, 8704−8713.
(28) Dattagupta, S.; Blume, M. *Phys. Rev. B* **1974**, *10*, 4540−4550.
(29) Zadrozny, J. M.; Atanasov, M.; Bryan, A. M.; Lin, C. Y.; Rekken, B. D.; Power, P. P.; Neese, F.; Long, J. R. *Chem. Sci.* **2013**, *4*, 125−138.